Families of spherical caps: spectra and ray limit

2008 J. Phys. A: Math. Theor. 41 075309

(http://iopscience.iop.org/1751-8121/41/7/075309)

IOP PUBLISHING JOURNAL OF PHYSICS A: MATHEMATICAL AND THEORETICAL

J. Phys. A: Math. Theor. **41** (2008) 075309 (25pp) doi:10.1088/1751-8113/41/7/075309

Families of spherical caps: spectra and ray limit

Niels Søndergaard[1] **and Thomas Guhr**[1,2]

[1] Division of Mathematical Physics, Lund University, LTH, Sweden
[2] Fachbereich Physik, Universität Duisburg-Essen, Germany

Received 26 September 2007, in final form 10 January 2008
Published 5 February 2008
Online at stacks.iop.org/JPhysA/41/075309

Abstract

We consider a family of surfaces of revolution ranging between a disc and a hemisphere, that is spherical caps. For this family, we study the spectral density in the ray limit and arrive at a trace formula with geodesic polygons describing the spectral fluctuations. When the caps approach the hemisphere the spectrum becomes equally spaced and highly degenerate whereas the derived trace formula breaks down. We discuss its divergence and also derive a different trace formula for this hemispherical case. We next turn to perturbative corrections in the wave number where the work in the literature is done for either flat domains or curved without boundaries. In the present case, we calculate the leading correction explicitly and incorporate it into the semiclassical expression for the fluctuating part of the spectral density. To the best of our knowledge, this is the first calculation of such perturbative corrections in the case of curvature and boundary.

PACS numbers: 03.65.Sq, 05.45.Mt

(Some figures in this article are in colour only in the electronic version)

1. Introduction

Waves can be approximated by rays by means of asymptotic expansions. For example in the design of optical lenses one always resorts to the equations describing the rays of light rather than the Maxwell equations for the electromagnetic waves. Similarly for the interpretation of earthquakes, one replaces elastic waves with curved rays.

The parameter of such an expansion for a classical wave phenomenon is the wave length divided by a typical geometrical scale of the systems. In optics, this leads from electromagnetic waves to rays of light. In quantum mechanics, however, the asymptotic parameter is $\hbar$ compared to a typical action of the system, that is, it involves a natural constant. Nevertheless on the formal mathematical level, the asymptotic expansions have the same character and many semiclassical results have their analogue for classical wave equations in terms of similar ray interpretations. Likewise, there are trends in the opposite direction, from classical waves to quantum mechanics, such as imaging by electron waves in e.g. photodetachment microscopy

[1]. For this paper we stress that the semiclassical discussion of a free quantum-mechanical particle on a curved surface is similar to that of the ray theory for a classical membrane. Thus, in curved spaces, the effect of geometry on quantum mechanics is that wave packets follow *geodesic motion* in the semiclassical limit in the absence of potentials [2]. Geodesics are curves which are stationary with respect to the length under variations.

In this contribution we consider an one-parameter family of spherical caps. We show that detailed information about the spectra is obtained from periodic geodesic orbits. In particular, we explain the drastic change in the spectrum involving a clustering effect when approaching the half-sphere by varying the opening angle of the cap. Besides the method of stationary phase, we shall use the asymptotic technique attributed to Jeffreys, Wentzel, Kramers and Brillouin and denote it by *JWKB*. We shall discuss how to take into account the effect of the boundary with respect to the first JWKB correction using the scattering approach of [3].

Our interest in spherical caps is motivated by the ongoing experimental efforts for elastic shell caps by Ellegaard and his group.

This paper is organized as follows: to aid a classical interpretation we recall various facts about geodesic polygons in section 2. Then the spectral problem is introduced in section 3 with a discussion of the asymptotics of the associated Legendre polynomials. Using a scattering approach to quantization, this allows a derivation of a trace formula for the density of states, see section 4. Then follows a discussion of the pure hemisphere in section 5 which can be solved exactly along with a comparison in section 6 with the previous general case. We include JWKB corrections in the trace formula in section 7. We end with a short discussion in section 8. Finally, calculational details are given in appendices.

2. Classical quantities: geodesic polygons

We fix the notation in section 2.1 and discuss the conservation of angular momentum during the geodesic flow in section 2.2. For reference later on, we compile a list of geometric quantities for geodesic polygons in section 2.3, give a condition for the inclination of a segment in a geodesic polygon in section 2.4 and discuss the concept of anholonomy present in systems with continuous symmetries such as $U(1)$ with a calculation for the case of the cap in section 2.5.

2.1. Notation

We shall consider a family of surfaces of revolution. Individual members of this family are spherical caps and are parameterized by a radius of curvature R and an opening angle θ_0 calculated from the axis of symmetry taken to be the z-axis, see figure 1. We consider caps ranging from almost a disc to a hemisphere and we restrict ourselves to caps with opening angles less than or equal to $\pi/2$. The singular cases corresponding to $\theta_0 = 0, \pi$ are not considered.

2.2. Conservation of angular momentum

If a surface possesses symmetries these influence the dynamics of the geodesic flow. For example, for surfaces of revolution Clairaut [4] found from the geodesic equations:

$$r \cos \Theta = \text{Cst.}, \tag{1}$$

where r is the radial distance from the rotation axis and Θ is the angle of the tangent vector of the geodesic with a given latitude, see [5]. When (1) is multiplied with the momentum p,

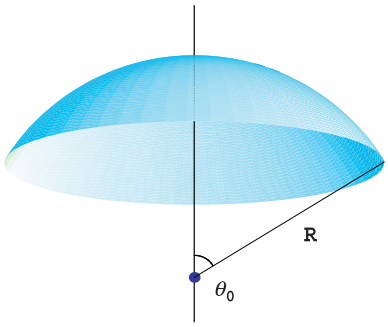

Figure 1. The cap geometry: opening angle θ_0 and curvature radius R.

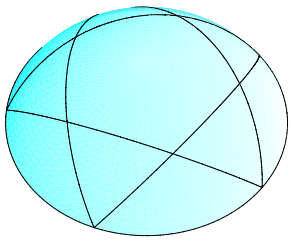

Figure 2. The pentagram orbit for opening angle $\theta_0 = \pi/3$.

the corresponding physical interpretation is that the angular momentum along the rotation axis is conserved. Here, one uses the fact that the momentum is conserved in the absence of potentials [2].

In the presence of a boundary, the geodesic flow is broken but it shall be continued by allowing geodesics to follow the law of reflection. Therefore, for the cap geometry the periodic orbits will be geodesic polygons composed of great circles. In the present case, the reflections are operations which preserve angular momentum.

Likewise, from a spectral point of view, the angular momentum is a good quantum number.

2.3. Geometrical orbit quantities

We label each geodesic polygon with n edges and winding number M[3] with a pair of numbers (n, M). The pentagram orbit for example has $(n, M) = (5, 2)$, see figure 2. Consider a single edge in such a polygon. Let its vertices be given in direction by the two unit vectors $\mathbf{e}_1$ and $\mathbf{e}_2$ with

$$\mathbf{e}_1 = \sin\theta_0\,\hat{\mathbf{x}} + \cos\theta_0\,\hat{\mathbf{z}} \tag{2}$$

and

$$\mathbf{e}_2 = \sin\theta_0\cos\delta\phi\,\hat{\mathbf{x}} + \sin\theta_0\sin\delta\phi\,\hat{\mathbf{y}} + \cos\theta_0\,\hat{\mathbf{z}}, \tag{3}$$

where the azimuthal angle traversed is denoted by

$$\delta\phi = \frac{2\pi M}{n}. \tag{4}$$

[3] i.e. how many times the orbit winds around the north pole.

So the angle from the origin between the two points defining the segment

$$\chi \equiv \angle(\mathbf{e}_1, \mathbf{e}_2) \tag{5}$$

can be found by e.g.

$$\cos\chi = \mathbf{e}_1 \cdot \mathbf{e}_2 = \cos^2\theta_0 + \sin^2\theta_0 \cos\frac{2\pi M}{n}. \tag{6}$$

Hence the length of this polygonal edge is

$$\Delta l = R\chi \tag{7}$$

corresponding to one nth of the total length of the orbit.

2.4. Orbit inclinations from conservation of angular momentum

With respect to the origin a particle moving on the segment with momentum p has an angular momentum $\mathbf{L}$. Classically $|\mathbf{L}|$ and L_z are conserved. The latter is also conserved under reflections from the boundary. The direction becomes

$$\hat{\mathbf{L}} = \frac{\mathbf{e}_1 \times \mathbf{e}_2}{|\mathbf{e}_1 \times \mathbf{e}_2|} \tag{8}$$

and the magnitude is

$$|\mathbf{L}| = Rp. \tag{9}$$

Using (2) and (3), we find after some calculation the projection of the angular momentum on the z-axis:

$$L_z = pR\cos\psi \tag{10}$$

with

$$\cos\psi = \frac{\sin\theta_0 \cos\frac{\pi M}{n}}{\sqrt{\cos^2\theta_0 + \sin^2\theta_0 \cos^2\frac{\pi M}{n}}}. \tag{11}$$

In the following, we shall interpret (11) as a condition fulfilled by an orbit's inclination (measured relative to the polar axis) when given winding number M, number of bounces n and the opening angle of the cap θ_0.

2.5. Anholonomy

We consider the geodesic flow as a dynamical system. We shall record the position of the trajectory at the boundary by a corresponding azimuthal angle ϕ and think of it as a phase. For an initial incidence angle this phase will change by constant discrete increments $\delta\phi$ and only if this phase is given by (4) the orbit is closed. We now enquire how this phase changes as the direction of the orbit changes. This direction we choose to be controlled by L_z, the classical variable conjugate to the azimuthal variable ϕ. Thus, if a general azimuthal increment $\delta\phi$ changes, L_z changes via (3), (6) and (10). After some calculation this yields

$$\frac{\partial\delta\phi}{\partial L_z} = -\frac{2}{pR}\frac{\left(\cos^2\theta_0 + \sin^2\theta_0 \cos^2\left(\frac{\delta\phi}{2}\right)\right)^{3/2}}{\sin\theta_0 \cos^2\theta_0 \sin\left(\frac{\delta\phi}{2}\right)} \tag{12}$$

the *phase lag* [15, 16], also called the anholonomy.

3. Semiclassics using asymptotics of Legendre polynomials

We have finished the classical considerations and will next study spherical caps using wave mechanics. First, we shall discuss the wave problem of a spherical surface and the corresponding symmetry-reduced problem given by Legendre's equation in section 3.1. We find the ray limit of this reduced wave equation using the JWKB method in section 3.2. This will lead to asymptotics for the associated Legendre polynomials.

3.1. Wave problem of scalar cap

The simplest model of cap vibrations corresponds to that of a quantized particle confined in the cap region:

$$(\Delta + k^2)\Psi = 0 \tag{13}$$

with Δ the curved Laplacian, k the wave number and specified boundary conditions such as Dirichlet $\Psi = 0$ or Neumann $\partial_n \Psi = 0$ at $\theta = \theta_0$. Equation (13) is also considered to describe curved drums.

When solving (13) by separation of variables using

$$\Psi = u(\theta)\, \mathrm{e}^{\mathrm{i}m\phi} \tag{14}$$

Legendre's equation

$$(1-x^2)\frac{\mathrm{d}^2 u}{\mathrm{d}x^2} - 2x\frac{\mathrm{d}u}{\mathrm{d}x} + \left(l(l+1) - \frac{m^2}{1-x^2}\right)u = 0 \tag{15}$$

arises with the variable $x = \cos\theta$ and the parameter

$$l(l+1) = (kR)^2 \equiv \kappa^2 \tag{16}$$

related to the spectrum. The regular solutions at $\theta = 0$ are given by the associated Legendre polynomials $P_l^m(x)$ whereas the irregular ones by $Q_l^m(x)$. Consequently, the Dirichlet solutions are the solutions of

$$P_l^m(x_0) = 0 \tag{17}$$

with respect to l and where $x_0 \equiv \cos\theta_0$, see figure 3 showing $\log\left(\left|P_l^m(x)\right|\right)$ in the case $m = 20$ and $\theta_0 = \pi/3$. When $l < m$ the dips show an integer spacing. There as m is an integer $P_l^m(x) = 0$ for all x and integer $l < m$, since in general at integer l, m the P_l^m is proportional to an mth derivative of an lth order polynomial. These 'roots' are indeed present in figure 3 up to $l = m - 1 = 19$, but do not correspond to genuine eigenmodes as the wavefunction is globally zero. Around $l \approx m$ there is a gap after which physical states appear spaced apart typically with a non-integer value for high l. The reason for this fixed spacing is due to the following asymptotics when $l \gg m$ [6]:

$$P_l^m(\cos\theta) = \frac{\Gamma(l+m+1)}{\Gamma\left(l+\frac{3}{2}\right)}(\pi \sin\theta)^{-1/2}\cos\left(\left(l+\frac{1}{2}\right)\theta - \frac{\pi}{4} + m\frac{\pi}{2}\right) + O(l^{-1}). \tag{18}$$

To further understand the roots of condition (17) in the interface region where l and m are comparable we turn to a more detailed asymptotics of the Legendre polynomials.

3.2. JWKB of Legendre polynomials

Standard tables of functions often discuss the asymptotics of $P_l^m(x)$ in the extreme cases where either $l \gg m$ or $m \gg l$. However, as mentioned we need the more interesting intermediate

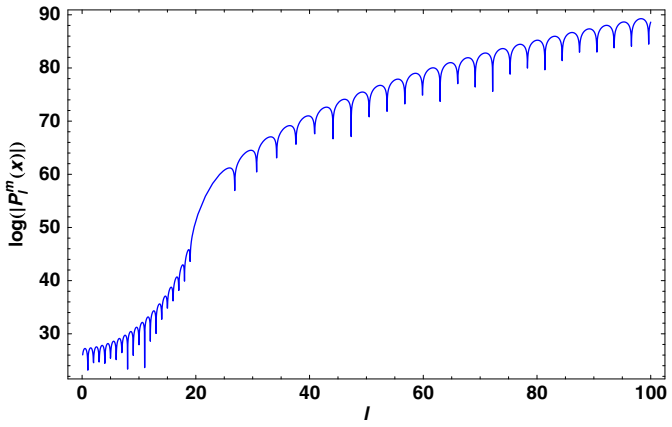

Figure 3. The values of $\log|P_l^m(x)|$ for $m = 20$ and $x = \cos(\pi/3)$. For $l > m$ the dips correspond to eigenmodes being roots of $P_l^m(x) = 0$, see section 3.1.

physical situation with both l and m large and their ratio well defined following [7] (more explanatory details can be found in [8–10]).

Thus, consider large angular momenta l and from that define a small parameter

$$\epsilon = (l(l+1))^{-1/2} \equiv \frac{1}{kR} \tag{19}$$

and demand that the z-component of the angular momentum m to be of the same asymptotic order as l. Hence, define the projected angular momentum on the z-axis respective x–y-plane

$$m = L_z \qquad \text{and} \qquad l_\perp = \sqrt{l(l+1) - m^2}. \tag{20}$$

The classical picture is the precession of the angular momentum around the z-axis at the angle ψ, where we defined the corresponding cosine in (11). Thus for semiclassics we shall associate a classical angle ψ to the quantum-mechanical angular momentum by

$$\cos\psi = \epsilon m \qquad \text{and} \qquad \sin\psi = \epsilon l_\perp \equiv a. \tag{21}$$

To simplify the following analysis, switch from the original wavefunction u to

$$w(x) \equiv \sqrt{1-x^2}\,u(x). \tag{22}$$

Then Legendre's equation (15) becomes

$$\epsilon^2 \frac{\mathrm{d}^2 w}{\mathrm{d}x^2} + \frac{a^2 - x^2 + \epsilon^2}{(1-x^2)^2} w = 0 \tag{23}$$

free from the first-order derivative term. This wave equation contains besides the kinetic term $w''(x)$ also potentials: in the notation of [11] the leading potential is Q with:

$$Q(x) = -\frac{a^2 - x^2}{(1-x^2)^2} \tag{24}$$

and a subdominant potential Q_2 proportional to ϵ^2

$$Q_2(x) = -\frac{1}{(1-x^2)^2}. \tag{25}$$

To leading order in the JWKB method this subdominant potential is dropped although we will also consider the effect of Q_2 later on.

First there is a momentum

$$p(x) = \sqrt{-Q(x)} = \frac{\sqrt{a^2 - x^2}}{1 - x^2}. \tag{26}$$

Second there is a turning point when this momentum vanishes, i.e. at $x = \pm a$. We only consider $0 < x_0 < x < a$.

4. Semiclassical scattering quantization

In the previous section we discussed the ray limit of the symmetry-reduced problem of a spherical cap in terms the asymptotics of the associated Legendre polynomials. In this section, this information is used to derive the corresponding full spectrum with a ray limit involving geodesic polygons. First, we state a simple asymptotic condition for an eigenmode in a form similar to that of Bohr–Sommerfeld quantization in section 4.1. Then, we reformulate the resonance condition as one arising from scattering in section 4.2 and check this condition numerically in section 4.3. We next progress from this condition for individual eigenfrequencies belonging to a given irreducible representation to the full spectral density in section 4.4. We find that the derived asymptotic density of states diverges in the limit of a hemisphere in section 4.5.

4.1. Resonance condition in the ray limit

Following steps similar to the usual for Bohr–Sommerfeld quantization [11] discussed in detail in appendix A, the Dirichlet condition $\Psi = 0$ gives the following JWKB condition for an eigenmode:

$$\frac{1}{\epsilon} I_0 + \frac{\pi}{4} = n\pi \tag{27}$$

for $n \in \mathbb{Z}$ and an *action* integral I_0 given as

$$I_0 = \int_{x_0}^{a} p(t)\,\mathrm{d}t = \int_{x_0}^{a} \frac{\sqrt{a^2 - t^2}}{1 - t^2}\,\mathrm{d}t = \operatorname{acos}\left(\frac{x_0}{a}\right) - \sqrt{1 - a^2}\operatorname{atan}\left(\frac{\sqrt{a^2 - {x_0}^2}}{\sqrt{1 - a^2}x_0}\right). \tag{28}$$

This condition follows from finding the roots of the asymptotic form of the wavefunction

$$u \sim Y_{lm}(\theta, \phi = 0) \approx \frac{1}{\pi}(a^2 - x^2)^{-1/4} \cos\left(\frac{I_0}{\epsilon} - \frac{\pi}{4}\right) \tag{29}$$

taken proportional to a spherical harmonic. We derive this leading asymptotic form in appendix A as well as perturbative corrections for the use later on in section 7.

4.2. Scattering formulation

We aim at deriving the spectral density for the spherical cap with the spectrum given by the condition (27) using ideas from scattering theory [3].

What is the scattering approach to quantization? This method exploits the connection between an exterior scattering problem and an associated interior resonator problem. Thus, if we force an obstacle from the exterior at an interior eigenfrequency the scattered wave experiences no phase shift; we shall see this explicitly in our case. The method is often referred to as an inside–outside duality. We will apply this method to find the spectral density for the interior cap vibration problem using information from corresponding scattering data. We proceed to our particular geometry. There, formal scattering for curved billiards on e.g.

the sphere has already been discussed in [12]. For concreteness, we discuss the explicit form of the scattering states in detail in appendix B.

Thus in terms of scattering theory, we shall say that a condition for an eigenmode is that the phase Θ_m :

$$\Theta_m \equiv \frac{2}{\epsilon} I_0 + \frac{\pi}{2} \tag{30}$$

has to equal zero modulo 2π

$$\Theta_m = 0 \qquad (\mathrm{mod}\, 2\pi). \tag{31}$$

First, (31) is formally equivalent to (27); second, the discussion in appendix B shows that there is an underlying set of scattering states with precisely the scattering phase Θ_m. So we define a scattering matrix diagonal in the azimuthal quantum number m

$$\mathbb{S} = (S_m)_{m\in\mathbb{Z}} \qquad \text{and} \qquad S_m = \exp(-\mathrm{i}\Theta_m). \tag{32}$$

Then an eigenmode occurs when the corresponding scattering problem is transparent [3]. The choice of sign in (32) agrees with treatments of the flat case, i.e. the disc [3, 13].

4.3. Numerical test

As an example, there is an eigenmode for $l = 99.642\,894\,578\,7050$ and $m = 70$ to good approximation for $\theta_0 = \pi/3$, i.e. $P_l^m(\cos\theta_0) \approx 0$. For these values of l and m we can find ϵ and a from (19) and (21). The corresponding semiclassical phase evaluates to $\Theta_m/(2\pi) = 4.0014$, close to an integer.

4.4. Spectral density

The distribution function for the eigenfrequencies is captured by the density of states. For convenience, instead of frequencies the spectral parameter in this section is the dimensionless wave number $\kappa = kR$. For several spectral problems the density can be approximated by a decomposition consisting of a smooth $\overline{\rho}$ and oscillating part $\tilde{\rho}$. The smooth part is the most studied [14] whereas less is known about the oscillatory part. For our system we turn the attention to the latter.

In the scattering formulation [3] the *fluctuating spectral density* becomes

$$\tilde{\rho}(\kappa) = -\frac{1}{\pi}\mathrm{Im}\sum_{n=1}^{\infty}\frac{1}{n}\frac{\partial}{\partial\kappa}\mathrm{Tr}\,(\mathbb{S}^n) = \frac{1}{\pi}\mathrm{Im}\sum_{n=1}^{\infty}\frac{1}{n}\frac{\partial}{\partial\kappa}\mathrm{Tr}\,(\mathbb{S}^{*n}). \tag{33}$$

The terms for the nth power in (33) correspond to orbits bouncing n times as we shall see in the following.

4.4.1. Poisson summation and nth trace. As the scattering matrix (32) is diagonal the trace becomes

$$\mathrm{Tr}\;\mathbb{S}^n = \sum_m (S_m)^n = \sum_m \exp(-\mathrm{i}n\Theta_m). \tag{34}$$

In the general case (34) is done by Poisson summation

$$\mathrm{Tr}\;\mathbb{S}^n = \sum_m (S_m)^n = \sum_M \int_{-\infty}^{\infty} \mathrm{d}m\, \exp(\mathrm{i}(-n\Theta_m - 2\pi m M)) \tag{35}$$

and subsequently approximated by stationary phase.

4.4.2. The stationary point corresponds to geodesic polygons. The saddle-point condition for the trace (35) becomes

$$-n\frac{\partial\Theta_m}{\partial m} = 2\pi M. \tag{36}$$

We calculate the derivative of (30) using (28)

$$\frac{\partial I_0}{\partial m} = -\epsilon \operatorname{atan}\left(\frac{\sqrt{a^2 - x_0^2}}{\sqrt{1-a^2}x_0}\right) = -\epsilon \operatorname{atan}\left(\frac{\sqrt{\sin^2\psi - \cos^2\theta_0}}{\cos\psi\cos\theta_0}\right) \tag{37}$$

and find the condition

$$\frac{\pi M}{n} = \operatorname{atan}\left(\frac{\sqrt{\sin^2\psi - \cos^2\theta_0}}{\cos\psi\cos\theta_0}\right) \tag{38}$$

or by elementary trigonometric manipulations

$$\cos\psi = \frac{\sin\theta_0\cos\frac{\pi M}{n}}{\sqrt{\cos^2\theta_0 + \sin^2\theta_0\cos^2\frac{\pi M}{n}}} \tag{39}$$

and

$$\sin\psi = \frac{\cos\theta_0}{\sqrt{\cos^2\theta_0 + \sin^2\theta_0\cos^2\frac{\pi M}{n}}}. \tag{40}$$

These conditions are precisely those of classical geodesic polygons winding M times around the north pole and hitting the boundary n times, see (11). For an example of a classical polygon orbit see figure 2 and figure 5 showing the pentagram orbit.

4.4.3. Action at stationary point. We next discuss the constant term in the stationary phase approximation of (35).

The square of the denominator of (40) is rewritten using (6):

$$\cos^2\theta_0 + \sin^2\theta_0\cos^2\frac{\pi M}{n} = \cos^2\theta_0 + \sin^2\theta_0\frac{1+\cos\left(\frac{2\pi M}{n}\right)}{2} = \frac{1+\cos\chi}{2} = \cos^2\frac{\chi}{2} \tag{41}$$

with χ being the angle of a single geodesic segment (5). Then consider

$$I_0 = \operatorname{acos}\left(\frac{\cos\theta_0}{\sin\psi}\right) - \frac{\pi M}{n}\cos\psi = \frac{\chi}{2} - \frac{\pi M}{n}\cos\psi \tag{42}$$

by (28), (40) and (6). We proceed to calculate $-n\Theta_m - 2\pi mM$ in (35) by (30): the $2\pi mM$ cancels with the remaining term from (42) by (21). Thus

$$-n\Theta_m - 2\pi mM = -n\frac{\chi}{\epsilon} - n\frac{\pi}{2}. \tag{43}$$

For the trace formula (33) eventually the conjugate scattering phase is used corresponding to minus (43). By (7), $n\chi/\epsilon = n\chi kR$ corresponds to the wave number times the total length of the geodesic polygon, i.e. the classical action of the geodesic polygon. At this point we identify the classical angular momentum Rp with multiples of the dimensionless wave mechanical, i.e. $\sqrt{l(l+1)}$, with pR replaced by kR.

4.4.4. Second variation. From (37) the second derivative becomes

$$\frac{\partial^2 I_0}{\partial m^2} = \epsilon^2 \frac{x_0}{a^2\sqrt{a^2 - x_0^2}} = \epsilon^2 \frac{\left(\cos^2\theta_0 + \sin^2\theta_0 \cos^2\frac{\pi M}{n}\right)^{3/2}}{\cos^2\theta_0 \sin\theta_0 \sin\frac{\pi M}{n}} \tag{44}$$

when evaluated at the saddle point.

We express this Hessian using the classical anholonomy:

$$\frac{\partial^2 I_0}{\partial m^2} = -\frac{\epsilon}{2}\frac{\partial \delta\phi}{\partial L_z} \tag{45}$$

when comparing (44) with (12). Such identifications are customary in the context of trace formulae for systems with continuous symmetries [15, 16].

As for the interpretation of the point of stationary phase in section 4.4.3, we identify the classical angular momentum in (45) with the dimensionless wave mechanical momentum kR. Alternatively, we could have chosen a dimensionless measure of orbit anholonomy with a particle of unit classical momentum: $\partial\delta\phi/\partial(\cos\psi)$, see (12).

4.4.5. Trace formula. Collecting the previous results leads to the following oscillatory density of states in the variable $\kappa = kR$:

$$\tilde{\rho}(\kappa) = \sqrt{\frac{2}{\pi}} \sum_{M=1}^{\infty} \sum_{n=1}^{\infty} \sqrt{\left|\frac{\partial L_z}{\partial \Delta\phi}\right|} \chi (-1)^n \cos\left(n\chi\kappa - n\frac{\pi}{2} + \frac{\pi}{4}\right). \tag{46}$$

We summarize the various factors in this formula. In particular χ being the angle of a segment from the origin, $n\chi\kappa = k \cdot nR\chi$ is the classical phase proportional to the length of the geodesic polygon. The sign $(-1)^n$ is the phase shift from the Dirichlet boundary condition. Furthermore, the derivative $\partial L_z/\partial\Delta\phi$ is interpreted as the accumulated phase lag for a closed orbit with n segments $\Delta\phi \equiv n\delta\phi$ using (12).

The result (46) for the density of states of the spherical cap is consistent with the general $U(1)$-symmetry-reduced trace formulae discussed in [15, 16]. Similar agreements are found in the flat case for a disc, both quantum and elastic [3, 17]. Equation (46) represents the result to leading order in κ. Later in section 7 we include the first perturbative correction.

The classical interpretation of the spectral density also holds more generally: much earlier in systems without symmetries Gutzwiller connected the fluctuations to classical periodic orbits [18] using the method of path integrals.

For an opening angle θ_0 larger than $\pi/2$ one can always associate the spectrum with that of a cap with opening angle $\pi - \theta_0$ as

$$0 = P_l^m(-x) = \pm P_l^m(x) \tag{47}$$

with $x = \cos\theta_0$, already remarked in [12]. In particular, the geodesic polygons of a small cap also govern the spectral fluctuations of its complementary cap.

Numerical checks: By including a few orbits and many repeats it is possible to build up a distribution with sharp peaks, see figure 4. This technique is discussed by e.g. [19] for the flat case of a disc. We have performed this simple test as a check for both Dirichlet and Neumann. In all cases at $\theta_0 = \pi/3$ the peaks fell approximately at the positions of the exact eigenfrequencies when including sufficiently many short orbits and repeats.

4.5. Analysis of orbits as the opening angle changes

We now consider the trace formula (46) for general opening angles and discuss what happens as the opening angle changes. As the opening angle is varied the set of periodic orbits changes

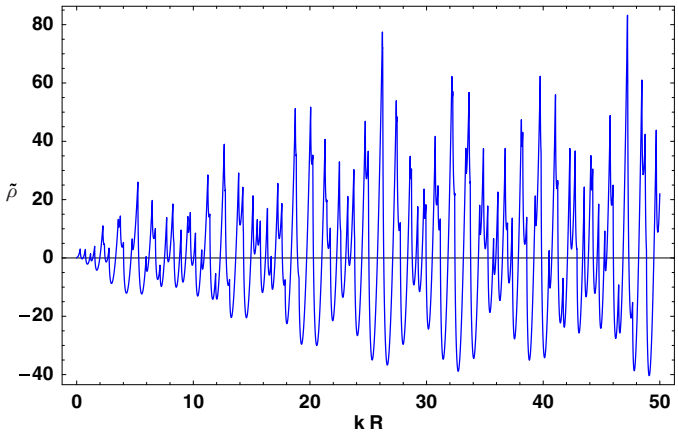

Figure 4. Spherical cap: oscillatory density of states for opening angle $\theta_0 = \pi/3$.

accordingly. Figure 5 shows how the pentagram orbit gradually converges from a pentagram in the plane towards an orbit going twice around the equator. Likewise the semiclassical weights associated with each orbit change, see figure 5. The calculations were done using the first 14 orbits having winding numbers (2, 1), (3, 1), ..., (9, 2), (9, 4) and up to 80 repeats.

Thus, the prefactor for each orbit family in the trace formula is $(\partial L_z/\partial\Delta\phi)^{1/2}$. Using (12) where $\delta\phi = \pi$, $\Delta\phi = 2\pi$ being the angular increments for the diameter orbit:

$$(kR)^{-1/2} \cdot \left(\frac{\partial L_z}{\partial \Delta\phi}\right)^{1/2}_{\text{diam}} = \frac{1}{2}\,\mathrm{d}\theta^{-1/2} + O(\mathrm{d}\theta^{3/2}). \tag{48}$$

On the other hand non-diameter orbits have weights going rapidly to zero as a function of the deficit in the opening angle:

$$(kR)^{-1/2} \cdot \left(\frac{\partial L_z}{\partial \Delta\phi}\right)^{1/2}_{\text{non-diam}} = O(\mathrm{d}\theta). \tag{49}$$

In conclusion, in the limit of the hemispherical cap the diameter orbit controls the spectral density. This will also show up in section 5.

5. The hemisphere

In the hemispherical case, the spectrum can be found exactly: we consider the spectrum in terms of individual levels in section 5.1 respective in the form of a spectral density in section 5.2.

5.1. Exact spectrum of hemisphere

For Dirichlet or Neumann conditions the eigenfunction in the polar variable either is odd or even. The parity of the Legendre polynomial is governed by

$$P_l^m(-x) = (-1)^{l-m} P_l^m(x). \tag{50}$$

Thus Dirichlet or Neumann conditions hold when either

$$l - m = \text{odd} \qquad \text{or} \qquad l - m = \text{even}. \tag{51}$$

with degeneracies $\nu_D = l$ respective $\nu_N = l + 1$. Thus the spectrum will display bunching of eigenmodes at integer l respective approximate half integer κ.

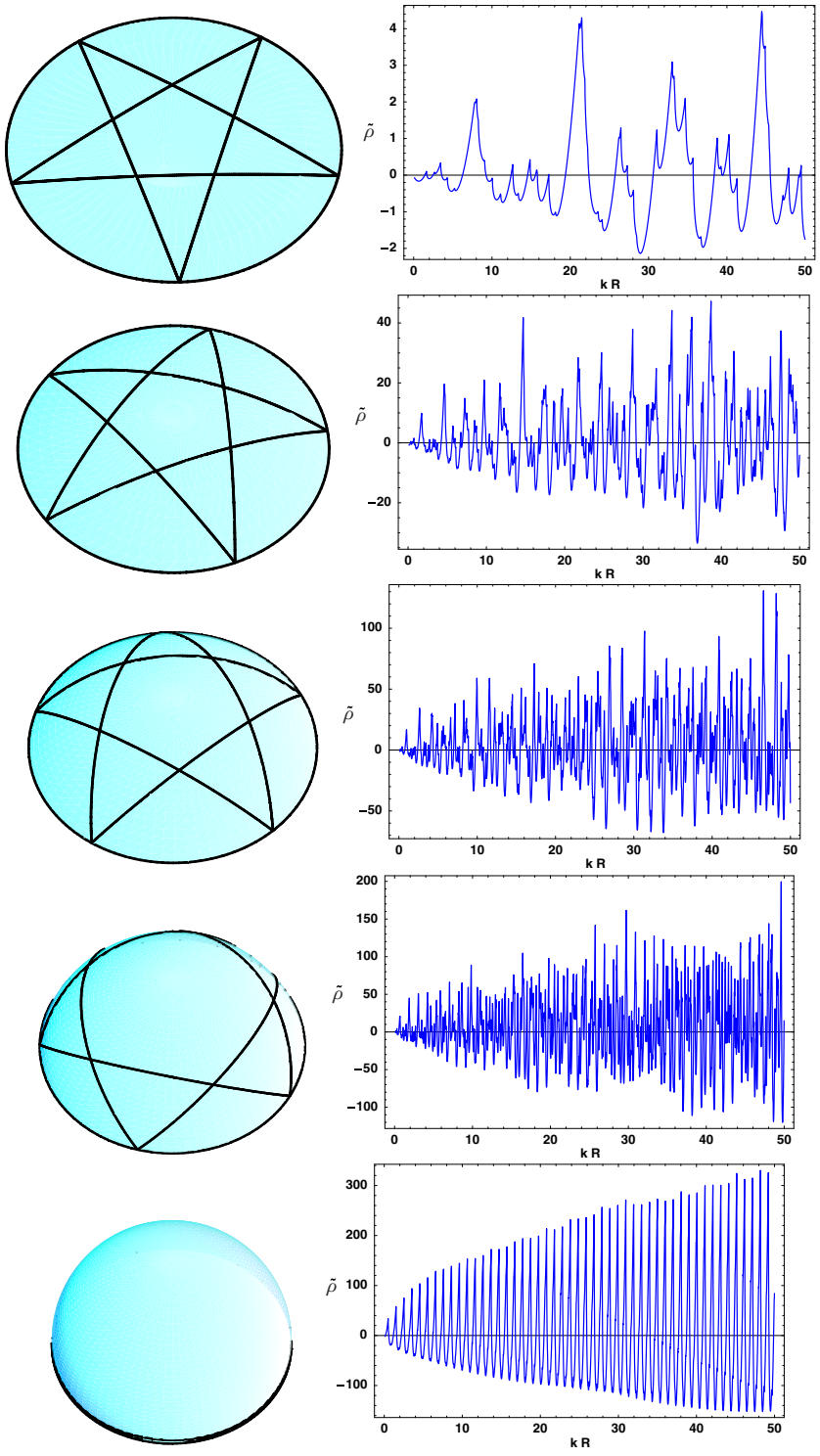

Figure 5. The pentagram orbit and the density of states for fixed radius ($R = 1$m) and varying opening angles $\theta_0 \in \{5.7^\circ, 26.5^\circ, 47.2^\circ, 68.0^\circ, 88.7^\circ\}$.

5.2. Hemisphere density of states

As we know the spectrum, the spectral density can likewise be written exactly. Denoting the degeneracy as ν the density becomes

$$\begin{aligned}\rho(l) &= \sum_{n=0}^{\infty} \nu(l)\delta(l-n) \\ &= \begin{cases} \sum_{n=0}^{\infty} l\delta(l-n) & \text{(Dirichlet)} \\ \sum_{n=0}^{\infty}(l+1)\delta(l-n) & \text{(Neumann).}\end{cases}\end{aligned}$$

Poisson summation then gives the density in the Dirichlet case

$$\begin{aligned}\rho_D(l) &= \sum_{N=-\infty}^{\infty} l\,\mathrm{e}^{\mathrm{i}2\pi Nl} + \frac{l}{2}\delta(l) \\ &= l + 2l\sum_{N=1}^{\infty}\cos(2\pi Nl)\end{aligned}$$

respective in the Neumann case

$$\begin{aligned}\rho_N(l) &= \sum_{N=-\infty}^{\infty} (l+1)\,\mathrm{e}^{\mathrm{i}2\pi Nl} + \frac{l+1}{2}\delta(l) \\ &= (l+1) + 2(l+1)\sum_{N=1}^{\infty}\cos(2\pi Nl) + \frac{1}{2}\delta(l).\end{aligned}$$

Switching to the spectral parameter $\kappa = kR = l + 1/2 + O(l^{-1})$ for which $\kappa\,\mathrm{d}\kappa = (l+1/2)\,\mathrm{d}l$ holds exactly gives

$$\rho_D(\kappa) \approx \kappa - \frac{1}{2} + 2\left(\kappa - \frac{1}{2}\right)\sum_{N=1}^{\infty}\cos\left(2\pi N\left(\kappa - \frac{1}{2}\right)\right) \tag{52}$$

and

$$\rho_N(\kappa) \approx \kappa + \frac{1}{2} + 2\left(\kappa + \frac{1}{2}\right)\sum_{N=1}^{\infty}\cos\left(2\pi N\left(\kappa + \frac{1}{2}\right)\right) + \frac{1}{2}\delta\left(\kappa - \frac{1}{2}\right). \tag{53}$$

The first two terms above give the smooth contribution to the density of states. Likewise the last terms correspond to the oscillatory part.

The smooth counting function $\overline{N}$ is the integrated density of states and becomes

$$\overline{N}_{D/N} = \frac{k^2R^2}{2} \mp \frac{kR}{2} \tag{54}$$

the first term being the available phase-space volume divided by $(2\pi)^2$ whereas the latter is the boundary correction well known from flat Helmholtz resonators $\mp k/(4\pi)L$ with L being the length [14, 20]. Their sum corresponds to the spectral density of a full sphere. In particular, the sum of the boundary corrections adds up to zero corresponding to no boundary.

The fluctuations are governed by the phase $2\pi N\kappa = k \cdot 2\pi RN$ of the Nth repeat of an orbit with length of the circumference $2\pi R$, see figure 6.

6. Comparing the two trace formulae

In sections 4.4.5 and 5.2 we presented two trace formulae for the oscillatory density of states for a spherical cap. In this section we compare these two formulae.

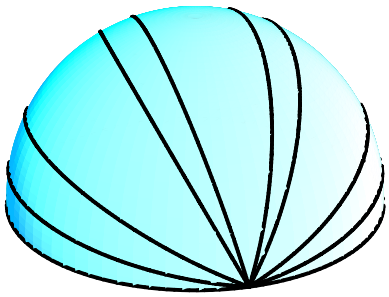

Figure 6. The hemisphere: orbits with the length of the perimeter.

Orbits. The first trace formula (46) derived for a general cap opening angle contains a countable infinite number of orbits whereas the second (52) only has a single orbit with the length of the perimeter.

Weight versus wave number. In the hemisphere case this orbit has a weight proportional to the spectral parameter and hence is of the order of the smooth part of the density. However, in the non-hemisphere case families of orbits have weights only proportional to the square root of the spectral parameter. This is the conventional result for families of orbits in two-dimensional systems.

Weight versus opening angle. Inspection of the first trace formula (46) in section 4.5 revealed that non-diameter orbits are assigned weights that vanish when the opening angle converges to $\pi/2$, i.e. that of a hemispherical cap. On the other hand, the diameter orbit has a weight which goes to infinity in this limit. In conclusion the first trace formula is a non-uniform asymptotic result valid for $0 < \theta_0 < \pi/2$. On the other hand the second trace formula is only valid at $\theta_0 = \pi/2$.

Near hemisphere. When the opening angle approaches $\pi/2$ (46) has been checked to reproduce the exact peak positions, $\kappa \approx l + 1/2$ with $l \in \mathbb{N}$: a little bit away e.g. $\theta_0 = 89.08^\circ$ is not sufficient whereas at e.g. $\theta_0 = 89.95^\circ$ the predicted half integers occur, see figure 7. This comparison was made at relatively high wave numbers with $\kappa = kR \approx 45$.

7. Leading correction

The previous calculations were all done to leading order in the expansion parameter proportional to the inverse wave number $\epsilon \equiv (kR)^{-1}$. We shall now ask what is the correction to these results in this expansion parameter. There are two points of interest: the individual sub-spectra for each m (section 7.1) and the total spectrum on the level of the trace formula (section 7.2).

Besides the general question of how to calculate JWKB corrections, we comment on why that could be of interest: one benefit of JWKB corrections is that these may increase the validity of the trace formulae further down in the spectrum. Ultimately JWKB corrections are believed to be particularly important in dimensions larger than 2 [3]. General results for corrections are known in the case without boundaries [21, 22] whereas only little is known with boundaries (planar Dirichlet/Neumann case [23]). By studying the spherical cap we will

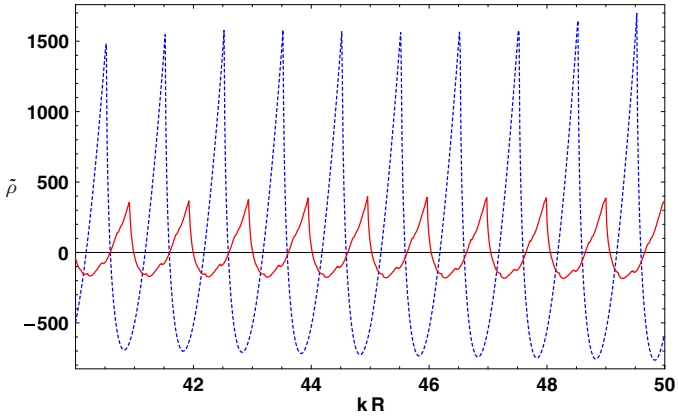

Figure 7. Semiclassical density of states. Full line: $\theta_0 = 89.08^\circ$ and dashed line: $\theta_0 = 89.95^\circ$.

get direct access to a simple situation for a curved manifold with boundary. In the present contribution we shall obtain a non-trivial result already for Dirichlet conditions.

7.1. Correction to leading asymptotics of associated Legendre polynomial

We are interested in the correction to the action I when going from the boundary x_0 to the turning point a for equation (23). The discussion of JWKB corrections when the orbit is between two turning points [11] is our starting point. We outline the corresponding theory below with details of the calculation given in appendix A. However, for (23) there is just a single turning point and now also the subdominant potential $Q_2(x)$ given by (25) not discussed in [11]. The way subdominant terms such as Q_2 enter is via the hierarchy of transport equations that arises in the JWKB method. To get the first correction the second or higher transport equations must be considered. In our case, Q_2 is present at the second transport equation.

In the typical case without boundary several results are known for subdominant corrections to the leading Hamiltonian. For instance [24] gives a systematic discussion of $\hbar$-corrections considering a general series expansion, the *Weyl symbol* of the corresponding Hamilton operator allowing for momentum terms as well. For a general reference on JWKB corrections see [25]. In our case, however, we must also consider the presence of a boundary x_0.

The result we find in appendix A is a second-order correction of the action

$$I \equiv I_0 + \epsilon^2 I_2, \tag{55}$$

where formally I_2 is found by integrating I_2' from the second transport equation. Just as the leading amplitude of the JWKB function determined by the first transport equation diverges near the turning point, also the second transport equation leads to divergences. In our case the subdominant potential Q_2 remains well behaved there. The singularities can be dealt with by for example transforming the problem to the Airy equation as in [11] and are given in detail in appendix A.

To state the final result for the phase I_2 we shall need the expansion of the potential Q in the coordinate x around the turning point a:

$$Q(x) \approx \alpha(x-a) + \beta(x-a)^2. \tag{56}$$

Thus in the transition region $x \approx a$ there is an approximate solution having the functional form of an Airy function which in the region $x < a$ takes the form of a sine function. That region also possesses a standard oscillatory JWKB solution

$$w_{osc}(x) \sim \mathrm{Im}[C \exp(\mathrm{i}I)] \tag{57}$$

with the action I calculated up to a point before the turning point ($a - \mu$ with $\mu \to 0+$)

$$I = I(x) = \int_x^{a-\mu} I'(t)\,\mathrm{d}t. \tag{58}$$

We next match this oscillatory solution to the regular Airy solution by adjusting the pre-factor C. This matching modifies the second-order phase to

$$I_2 \equiv \lim_{\mu\to 0+}\left(-\frac{5Q'(x_0)}{48(-Q(x_0))^{3/2}} + \frac{1}{48}\int_{x_0}^{a-\mu}\frac{Q''(t)}{(-Q(t))^{3/2}}\,\mathrm{d}t - \frac{\beta\alpha^{-3/2}}{12\sqrt{\mu}} - \frac{1}{2}\int_{x_0}^{a}\frac{Q_2(t)}{(-Q(t))^{1/2}}\,\mathrm{d}t\right). \tag{59}$$

The first three terms are stated in [11] whereas the final term is the correction from the subdominant potential Q_2. In (59), the first two terms and the last correspond to the result obtained by formally integrating the second transport equation for I_2 and doing a partial integration, see appendix A . In this context, the second term diverges as $Q(x)$ has a zero at the turning point. Given the expansion of $Q(x)$ by (56), the third term coming from the matching exactly cancels this divergence and can be thought of as a regularization.

Using computer algebra and further manipulations (59) reduces in the present case to

$$I_2 = \frac{x_0\left(3a^4 + 2\left(x_0^2 - 3\right)a^2 + x_0^2\right)}{24a^2\left(a^2 - x_0^2\right)^{3/2}} + \frac{\pi}{16} - \frac{1}{8}\mathrm{atan}\left(\frac{x_0}{\sqrt{a^2 - x_0^2}}\right). \tag{60}$$

For an analytical check of the phase in the case of $x_0 = 0$ see appendix A.

As a numerical example, we continue that of the end of section 4 with $l = 99.642\,894\,578\,7050$, $m = 70$ and $\theta_0 = \pi/3$. Including the correction I_2 for the action leads to a scattering phase in units of 2π: $\Theta_m/(2\pi) = 3.999\,993$. Further numerical checks are given in appendix A.3.3.

7.2. Effect of correction on the trace formula

The effect of the subdominant potential is to alter the saddle-point position m_0 to

$$m^* = m_0 + \epsilon^2 m_2 \tag{61}$$

to second order but this only affects the phases to fourth order: put

$$S = 2n(I_0 + \epsilon^2 I_2) \equiv S_0 + \epsilon^2 S_2. \tag{62}$$

Then as the original phase function is stationary

$$S_0^* = S_0(m_0) + (\partial_m S_0(m_0))\epsilon^2 m_2 + O(\epsilon^4) = S_0^* + O(\epsilon^4), \tag{63}$$

whereas the new part leads to

$$S_2^* = \epsilon^2 S_2(m_0). \tag{64}$$

Finally, there is a contribution coming from a saddle-point correction of the original integral, i.e. by expanding to fourth order in m around m_0, $S_0^{(4)}$. There are also other fourth order moments. However, these are of lower order in ϵ and can be neglected.

At the point of stationary phase

$$\int \mathrm{d}m \exp(-\mathrm{i}n\Theta_m) = \int \mathrm{d}m \exp\left(-\mathrm{i}\frac{S}{\epsilon}\right)$$
$$\approx \left(\frac{2\pi\epsilon}{|S_0''|}\right)^{1/2} \exp\left(\mathrm{i}n\frac{\pi}{2} - \mathrm{i}\frac{\pi}{4}\right) \exp\left(-\mathrm{i}\left(\frac{S_0}{\epsilon} + \epsilon S_2\right)\right) \exp\left(\sqrt{\mathrm{i}\epsilon}\frac{S_0^{(4)}}{8S_0^{(2)2}}\right). \quad (65)$$

For a given orbit family, the factor S_2 only alters the phase whereas the latter factor also alters both modulus and phase.

The density of states is calculated using (33): essentially a derivative with respect to $\kappa = 1/\epsilon$ is performed on (65). Furthermore, the derivatives of the action coefficients S_i are pertaining to m and for these

$$\frac{\partial}{\partial m} = -\epsilon^2 \frac{m}{a}\frac{\partial}{\partial a}. \quad (66)$$

In particular $S_0'' \sim \epsilon^2$. Thus apart from factors

$$\mathrm{Tr}\ \mathbb{S}^n \sim \epsilon^{-1/2} \exp\left(-\mathrm{i}\left(\frac{S_0}{\epsilon} + S_2\epsilon\right) + \xi\epsilon\right) \quad (67)$$

with

$$\xi = \alpha_1 + \mathrm{i}\alpha_2 \qquad \text{and} \qquad \alpha_1 = \alpha_2 = \frac{1}{\sqrt{28}}\frac{S_0^{(4)}}{S_0^{(2)2}}. \quad (68)$$

Hence the perturbative correction to the density of states goes as

$$\widetilde{\rho}(\kappa) \sim \partial_\kappa(\mathrm{Tr}\,\mathbb{S}^{*n}) \sim \sqrt{\kappa}S_0 \exp\left(\frac{\alpha_1}{\kappa}\right) \cos\left(\kappa S_0 + \frac{\Delta S}{\kappa}\right), \quad (69)$$

where

$$\Delta S = S_2 - \alpha_1 - \frac{1}{2S_0}. \quad (70)$$

Incorporating all pre-factors and constants yields

$$\widetilde{\rho}(\kappa) = \sqrt{\frac{2}{\pi}} \sum_{M=1}^{\infty}\sum_{n=1}^{\infty} \sqrt{\left|\frac{\partial L_z}{\partial \Delta\phi}\right|}\chi(-1)^n \exp\left(\frac{\alpha_1}{\kappa}\right) \cos\left(n\chi\kappa - n\frac{\pi}{2} + \frac{\pi}{4} + \frac{\Delta S}{\kappa}\right). \quad (71)$$

From (62) we note the dependence on the number of repeats in the $S_i \sim n$. Therefore $\Delta S = S_2 + O(n^{-1})$, so $S_2 = 2nI_2$ with I_2 given by (60) in the case of the spherical cap remains the most important for high repeats.

8. Summary and discussion

We derived a trace formula for the spectral fluctuations of a spherical cap of general opening angle. The fluctuations in the spectral density were found to be governed by geodesic polygons. The method used is based on scattering referred to as inside–outside duality with a discussion of the explicit scattering states. Next the exact case of a hemisphere was introduced and there the spectral fluctuations were found to be governed by a single orbit of stronger weight than in the non-hemisphere case. The leading result for general opening angles was compared to the hemispherical case at relatively high wave numbers $kR \approx 45$. Although non-uniform in nature, the general trace formula without JWKB correction in the limit of opening angles close to $\pi/2$ also exhibits peaks at positions corresponding to the hemispherical cap's density of states. Finally, the leading JWKB correction was discussed and incorporated.

We used the inside–outside duality in the derivation of the trace formula. The scattering states needed for this are perhaps not so familiar to physicists but these functions have already been introduced in seismology [9]. Furthermore inside–outside duality for billiards in curved spaces has been discussed recently in the thesis [12]. Despite that inside–outside duality is just one possible method for this problem of a spherical cap, it should also be mentioned that the method allows for generalizations and clear interpretations in more complicated cases such as systems of partial differential equations.

Thus, although the leading result for the spectral density in principle can be obtained by a general theory of symmetry reduced trace formulae by [15, 16] it is not always obvious how to generalize these results in applications for wave equations different from the Schrödinger equation: which reflection coefficients to use and what is the proper concept of the anholonomy entering for the overall amplitude of a family of orbits in the presence of for example ray-splitting. By construction, the scattering formalism automatically yields unitary reflection coefficients related to for example probability or energy flux. Furthermore, for the present work we have used the scattering method as a vehicle to go beyond the leading results and incorporate JWKB corrections. In particular, such corrections to the spectral density cannot at present be obtained from the works of [15, 16] which pertain to the leading result only. We should also mention that the scattering method can be extended to general shapes without symmetries by considering the scattering of suitable exterior states by for example attaching wave-guiding leads [3].

We expect the scattering method on spheres as discussed in this paper and [12] could be generalized to the case of a sphere with multiple circular holes. Here, addition formulae for the Legendre polynomials for non-integer angular momentum l [26] would lead to multiple-scattering expansions similar to those in flat space between discs or spheres [27].

As mentioned the work in this paper has partly been motivated by Ellegaard's experiments on elastic shell caps. His group has studied plates and three-dimensional elastic resonators (see [28–30]) but is at the present time of writing investigating shells as well. In this context, the work in this article on the curved scalar Helmholtz equation and those in the flat case [17, 31, 32] for two-dimensional elasticity show that derivations of trace formulae in more general settings are possible. Thus the combined case of curved elasticity [33], i.e. elastic shell caps, is indeed one generalization.

Acknowledgments

We thank the Swedish Research Council for financial support. One of us (TG) also acknowledges support from the Deutsche Forschungsgemeinschaft (Sonderforschungsbereich Transregio 12).

Appendix A. The JWKB solution

A.1. Hierarchy of JWKB equations

Using the oscillatory ansatz

$$w = C \exp\left(\mathrm{i}\left(\frac{I_0}{\epsilon} + I_1 + I_2\epsilon\right)\right) \tag{A.1}$$

for the second-order ordinary differential equation in the notation of [11]

$$\epsilon^2 w'' = (Q + Q_2\epsilon^2)w \tag{A.2}$$

gives the eikonal equation

$$(I_0')^2 + Q = 0 \tag{A.3}$$

and the transport equation:

$$-2I_1'I_0' + \mathrm{i}I_0'' = 0 \tag{A.4}$$

respective the second transport equation

$$-2I_2'I_0' + \mathrm{i}I_1'' - (I_1')^2 - Q_2 = 0 \tag{A.5}$$

containing the correction from the subdominant potential.

A.2. Leading order

We fix the action I_0 by integrating between x and the turning point a with the result (28). Likewise $I_1 = \mathrm{i}\log(-Q)^{1/4}$. From (A.1) and (22), a real JWKB solution in the oscillatory region away from the turning point is given up to two unknown constants A and δ as

$$u = A(1-x^2)^{1/2}(-Q)^{-1/4}\cos\left(\frac{I_0}{\epsilon}+\delta\right) = A(a^2-x^2)^{-1/4}\cos\left(\frac{I_0}{\epsilon}+\delta\right) \tag{A.6}$$

where A is an overall amplitude and δ is a phase shift.

One way of fixing A and δ is by matching the wavefunction to an exact solution, here taken as $\pi Y_l^m(\theta, \phi = 0)$ with

$$Y_l^m(\theta, \phi = 0) = (-1)^m\sqrt{\frac{2l+1}{4\pi}}\sqrt{\frac{\Gamma(l-m+1)}{\Gamma(l+m+1)}}P_l^m(\cos\theta), \tag{A.7}$$

at the point $x = 0$ [8, 26] using:

$$P_l^m(0) = \frac{2^m}{\pi^{1/2}}\frac{\Gamma\left(\frac{l+m+1}{2}\right)}{\Gamma\left(\frac{l-m+2}{2}\right)}\cos\left(\frac{\pi}{2}(l+m)\right) \tag{A.8}$$

and

$$P_l^{m\prime}(0) = \frac{2^{m+1}}{\pi^{1/2}}\frac{\Gamma\left(\frac{l+m+2}{2}\right)}{\Gamma\left(\frac{l-m+1}{2}\right)}\sin\left(\frac{\pi}{2}(l+m)\right). \tag{A.9}$$

To proceed with the match, the gamma functions in the normalization of the spherical harmonics are expressed via the duplication formula [6]:

$$\Gamma(2z) = \frac{1}{\sqrt{2\pi}}2^{2z-1/2}\Gamma(z)\Gamma\left(z+\frac{1}{2}\right) \tag{A.10}$$

and subsequently ratios of gamma functions are approximated with

$$\frac{\Gamma(z+a)}{\Gamma(z+b)} \approx z^{a-b} \tag{A.11}$$

valid for large z, see [6]. As in the main text l and m are assumed asymptotically large with a fixed ratio.

Next, the leading semiclassical phase at $x = 0$ evaluates to

$$I_0 = \frac{\pi}{2}(1-\cos\psi), \tag{A.12}$$

which together with $1/\epsilon \approx l + 1/2$ enters for the shift δ. Finally $\cos\psi/\epsilon \equiv m$ to all orders by definition (21).

Thus, for $A \equiv 1$ and $\delta \equiv -\pi/4$ the wavefunction matches

$$u \approx \pi Y_{lm}(\theta, \phi = 0). \tag{A.13}$$

In particular, the condition for an eigenmode is

$$\frac{I_0}{\epsilon} - \frac{\pi}{4} = \frac{\pi}{2} + n\pi \tag{A.14}$$

for $n \in \mathbb{Z}$.

A.3. The first correction

We turn to the case where the sub-leading phase I_2 is included. We distinguish between the oscillatory region (*osc*), the transition region (*trans*) and the decaying region (*exp*). We shall not be concerned with the decaying region discussed in detail in [11] (chapter 10.7). Instead, we focus on the oscillatory case from which it will be clear that the subdominant potential Q_2 can be included in the discussion as well.

A.3.1. Phase. We first remark that we can always relate the solution at the boundary point x_0 with that at x close to the turning point. The connection is by multiplication of the JWKB factor

$$w_{\mathrm{osc}}(x_0) = \mathrm{Im}\left[\exp(\mathrm{i}\Delta I(x_0, x))w_{\mathrm{osc}}(x)\right] \tag{A.15}$$

with

$$\Delta I(x, x_0) \equiv \int_{x_0}^{x} \mathrm{d}s \frac{\mathrm{d}I}{\mathrm{d}s}. \tag{A.16}$$

Thus eventually all actions are continued further to the boundary as in (59).

Hence, the transport equations can be integrated formally, at least outside the transition region, whereas these diverge at the turning point and require discussion. In detail, to get the action to first order in ϵ we need to integrate

$$\begin{aligned} I_2' &= -\frac{Q_2}{2(-Q)^{1/2}} + \frac{Q''}{8(-Q)^{3/2}} + \frac{5}{32}\frac{Q'^2}{(-Q)^{5/2}} \\ &= -\frac{Q_2}{2(-Q)^{1/2}} + \frac{Q''}{48(-Q)^{3/2}} + \frac{5}{48}\frac{\mathrm{d}}{\mathrm{d}x}\left(\frac{Q'}{(-Q)^{3/2}}\right) \end{aligned} \tag{A.17}$$

as follows from (A.5) with $I_0' = +(-Q)^{1/2}$ and $I_1' = \mathrm{i}(\log(-Q))'/4$ after some calculation. But, when this is integrated from x up to $a - \mu$ (with $\mu \to 0+$) the last two terms diverge algebraically with respect to μ.

We turn to the region near the turning point. The oscillatory solution is written in complex form as

$$w_{\mathrm{osc}}(x) \equiv C \exp\left(\mathrm{i}\int_{x}^{a-\mu} \mathrm{d}s I'(s)\right) \tag{A.18}$$

We shall expand in the distance from the turning point

$$\Delta x = x - a \tag{A.19}$$

with $\Delta x < 0$ corresponding to the oscillatory region. Thus from (56)

$$-Q = |\Delta x|\alpha\left(1 - \frac{\beta}{\alpha}|\Delta x|\right). \tag{A.20}$$

The leading action I_0 is found from

$$(-Q)^{1/2} \sim |\Delta x|^{1/2}\alpha^{1/2}\left(1 - \frac{\beta}{2\alpha}|\Delta x|\right) \tag{A.21}$$

so

$$\int_{\Delta x}^{0} \mathrm{d}s(-Q)^{1/2} \sim \alpha^{1/2}\left(\frac{2}{3}|\Delta x|^{3/2} - \frac{\beta}{5\alpha^{1/2}}|\Delta x|^{5/2}\right) \tag{A.22}$$

The next action I_1 is imaginary and contributes to the amplitude of the JWKB function with the factor

$$(-Q)^{-1/4} \sim |\Delta x|^{-1/4}\alpha^{-1/4}\left(1 + \frac{1}{4}\frac{\beta}{\alpha}|\Delta x|\right). \tag{A.23}$$

The second-order action I_2 follows from integration of (A.17). First,

$$\frac{Q''}{48(-Q)^{3/2}} \sim \frac{\beta}{24\alpha^{3/2}}|\Delta x|^{-3/2} \tag{A.24}$$

so

$$\int_{x}^{a-\mu} \mathrm{d}s\left(\frac{Q''}{48(-Q)^{3/2}}\right) \sim \frac{\beta}{12\alpha^{3/2}}(\mu^{-1/2} - |\Delta x|^{-1/2}). \tag{A.25}$$

Second, the exact term given by a derivative becomes

$$\frac{5}{48}\int_{x}^{a-\mu} \mathrm{d}s\frac{\mathrm{d}}{\mathrm{d}s}\left(\frac{Q'}{(-Q)^{3/2}}\right) \sim \frac{5}{48}\alpha^{-1/2}(\mu^{-3/2} - |\Delta x|^{-3/2}). \tag{A.26}$$

Finally, the subdominant potential term with $Q_2 = \gamma + O(\Delta x)$ (not having a zero at the turning point) becomes

$$-\frac{Q_2}{2(-Q)^{1/2}} \sim -\frac{\gamma}{2\alpha^{1/2}}|\Delta x|^{-1/2} \tag{A.27}$$

and leads to the regular

$$\int_{x}^{a-\mu} \mathrm{d}s\left(-\frac{Q_2}{2(-Q)^{1/2}}\right) \sim \frac{\gamma}{\alpha}(|\Delta x|^{1/2} - \mu^{1/2}). \tag{A.28}$$

On the other hand, in the transition region $x \approx a$ with $x < a$ there is also a solution w_{trans} in the form of the Airy function([11]: formula (10.7.7)). The Airy form is recognized in (A.2) by the transformation

$$x - a = \epsilon^{2/3}\alpha^{-1/3}t. \tag{A.29}$$

Then a perturbed Airy equation arises

$$\frac{\mathrm{d}^2 w_{\mathrm{trans}}}{\mathrm{d}t^2} = (t + \epsilon^{2/3}\alpha^{-4/3}\beta t^2)w_{\mathrm{trans}}. \tag{A.30}$$

The leading perturbation due to Q is included whereas that from Q_2 does not play a role at this order. Consequently

$$w_{\mathrm{trans}} \sim D\left(1 - \frac{\beta x}{5\alpha}\right)\mathrm{Ai}\left(\alpha^{1/3}\epsilon^{-2/3}\left(x + \frac{\beta x^2}{5\alpha}\right)\right). \tag{A.31}$$

We now expand this Airy function in the region $x < a$ to second order in an asymptotic series of oscillatory form:

$$\mathrm{Ai}(-z) \sim \sin\left(\zeta + \frac{\pi}{4}\right) - \frac{5}{48}z^{-3/2}\cos\left(\zeta + \frac{\pi}{4}\right) \approx \sin\left(\zeta + \frac{\pi}{4} - \frac{5}{48}z^{-3/2}\right) \tag{A.32}$$

for large z with

$$z = \alpha^{1/3}\epsilon^{-2/3}|\Delta x|\left(1 - \frac{\beta|\Delta x|}{5\alpha}\right) \tag{A.33}$$

and

$$\zeta = \frac{2}{3}z^{3/2} \sim \frac{2}{3}\alpha^{1/2}\epsilon^{-1}|\Delta x|^{3/2}\left(1 - \frac{3\beta|\Delta x|}{10\alpha}\right). \tag{A.34}$$

Calculations similar to those for w_{osc} give

$$w_{\mathrm{trans}}(x) \sim \mathrm{Im}\left[D\sqrt{\pi}\left(1 + \frac{\beta|\Delta x|}{4\alpha}\right)\epsilon^{1/6}\alpha^{-1/12}|\Delta x|^{-1/4}\exp\left(\mathrm{i}\left(\frac{2}{3}\alpha^{1/2}\epsilon^{-1}\left(|\Delta x|^{3/2} - \frac{3\beta|\Delta x|^{5/2}}{10\alpha}\right)\right.\right.\right.$$
$$\left.\left.\left. + \frac{\pi}{4} - \frac{5}{48}|\Delta x|^{-3/2}\alpha^{-1/2}\epsilon\left(1 + \frac{3\beta|\Delta x|}{10\alpha}\right)\right)\right)\right]. \tag{A.35}$$

This result for w_{trans} is matched with the previous oscillatory form w_{osc}. First, we note that provided we neglect terms of order $\epsilon|\Delta x|^{-1/2}$ there is a complete match in functional form with respect to $|\Delta x|$ in the oscillatory region close to the turning point. In particular, Q_2 does not play a role in the matching at this order. Second, as w_{trans} is independent of μ all dependence on μ must be removed in w_{osc}. This is done by adjusting the pre-factor C of the standard JWKB solution $w_{\mathrm{osc}} = \mathrm{Im}(C\exp(\mathrm{i}I))$. In this way singular terms in μ are absorbed. Thus for example also the last term's singularity in (A.17) proportional to $\mu^{-3/2}$ is removed.

Still in our case, the contribution from the subdominant Q_2 to the second correction to the phase is regular and eventually gives a correction to the result stated in [11] for the full phase (i.e. all the way to the boundary x_0):

$$\Delta I_2 = -\frac{1}{2}\int_{x_0}^{a}\frac{Q_2(s)}{I_0'(s)}\,\mathrm{d}s = -\frac{1}{2}\int_{x_0}^{a}\frac{Q_2(s)}{(-Q(s))^{1/2}}\,\mathrm{d}s. \tag{A.36}$$

Likewise the integration of the remaining terms in (A.17) is seen to correspond to those given in (59).

By construction the phase is now correct to first order in ϵ. This can be verified at the point $x = 0$ as follows: there the phase I_2 given by (60) evaluates to

$$I_2 = \frac{\pi}{16}. \tag{A.37}$$

However, using

$$\epsilon = l^{-1} - \frac{1}{2}l^{-2} + O(l^{-3}) \qquad \text{and} \qquad 1/\epsilon = l + \frac{1}{2} - \frac{1}{8}l^{-1} + \frac{1}{16}l^{-2} + O(l^{-3}) \tag{A.38}$$

and (A.12) as well as (21) on the oscillatory part

$$\begin{aligned}\psi &\propto \cos\left(\frac{I_0}{\epsilon} + I_2\epsilon - \frac{\pi}{4}\right) = \cos\left(\frac{\pi}{2}(l-m) + O(l^{-3})\right)\\ &\propto Y_{lm}(\theta = \pi/2, 0) + O(l^{-3})\end{aligned} \tag{A.39}$$

shows the agreement in the phase even to second order in l^{-1}. For further numerical checks see appendix A.3.3.

A.3.2. Amplitude. Even though our main interest is a JWKB-resonance condition which only depends on the phase we note that similar calculations are possible for the amplitude function. These show agreement between the JWKB result and the exact to first order l^{-1}.

Table A1. Scattering phase in units of 2π: the relative deviation from integer (A.40) at $\theta_0 = \pi/3$.

m	l	Leading	Corrected	m	l	Leading	Corrected
0	1.777	-9.43×10^{-3}	-1.01×10^{-3}	8	21.94	-5.77×10^{-5}	-1.81×10^{-6}
0	19.75	-1.32×10^{-4}	-2.93×10^{-7}	8	40.31	-3.73×10^{-5}	-4.37×10^{-8}
0	37.75	-3.76×10^{-5}	-2.36×10^{-8}	9	26.40	-5.28×10^{-5}	-7.20×10^{-7}
1	3.196	-3.79×10^{-3}	-6.68×10^{-4}	10	18.14	6.75×10^{-4}	-3.30×10^{-5}
1	21.24	-1.22×10^{-4}	-2.45×10^{-7}	10	37.00	-3.95×10^{-5}	-1.05×10^{-7}
1	39.24	-3.61×10^{-5}	-2.12×10^{-8}	11	29.08	-2.42×10^{-5}	-7.19×10^{-7}
2	7.622	-8.31×10^{-4}	-3.39×10^{-5}	12	20.68	8.30×10^{-4}	-3.29×10^{-5}
2	25.71	-8.69×10^{-5}	-1.30×10^{-7}	12	39.74	-3.06×10^{-5}	-1.05×10^{-7}
2	43.73	-2.99×10^{-5}	-1.46×10^{-8}	13	31.74	4.69×10^{-8}	-7.18×10^{-7}
3	8.991	-4.80×10^{-4}	-3.35×10^{-5}	13	34.88	-1.89×10^{-5}	-3.39×10^{-7}
3	27.16	-8.00×10^{-5}	-1.21×10^{-7}	15	24.46	1.01×10^{-3}	-3.27×10^{-5}
3	45.20	-2.87×10^{-5}	-1.37×10^{-8}	16	21.99	6.61×10^{-3}	-6.23×10^{-4}
4	19.53	-1.51×10^{-4}	-7.47×10^{-7}	17	23.21	6.72×10^{-3}	-6.22×10^{-4}
4	37.64	-4.23×10^{-5}	-3.33×10^{-8}	18	24.42	6.82×10^{-3}	-6.21×10^{-4}
5	17.87	-1.58×10^{-4}	-1.83×10^{-6}	19	29.45	1.17×10^{-3}	-3.25×10^{-5}
5	36.06	-4.67×10^{-5}	-4.65×10^{-8}	20	34.22	3.81×10^{-4}	-5.93×10^{-6}
6	16.14	-9.84×10^{-5}	-6.02×10^{-6}	21	38.87	1.59×10^{-4}	-1.80×10^{-6}
6	34.47	-5.11×10^{-5}	-6.86×10^{-8}	23	34.40	1.29×10^{-3}	-3.23×10^{-5}
7	20.59	-8.76×10^{-5}	-1.81×10^{-6}	25	36.86	1.34×10^{-3}	-3.22×10^{-5}
7	38.91	-4.03×10^{-5}	-4.44×10^{-8}	28	36.46	7.48×10^{-3}	-6.14×10^{-4}

A.3.3. JWKB phase at eigenmodes. Table A1 (opening angle $\theta_0 = \pi/3$) shows the deviation of the JWKB-scattering phase Θ measured in units of 2π from the nearest integer (denoted by $[\Theta/2\pi]$) normalized with that integer, i.e.

$$\frac{\Theta/2\pi - [\Theta/2\pi]}{[\Theta/2\pi]}. \tag{A.40}$$

Apart from the value at $(m, l) = (13, 31.74)$ an overall improvement is observed.

Appendix B. Scattering states

B.1. Exact scattering states

One possible set of exact scattering states for the sphere $\mathcal{S}^2$ are those used extensively in geophysics under the name traveling waves in the discussion of the Green's function and associated surface waves [9]. We define them normalized:

$$\psi_l^{(\pm)m} = \sqrt{\frac{\Gamma(l-m+1)}{\Gamma(l+m+1)}} \left(P_l^m(x) \mp \mathrm{i}\frac{2}{\pi} Q_l^m(x) \right) \exp(\mathrm{i}m\phi). \tag{B.1}$$

The opposite sign in (B.1) will be explained in the following.

With this choice each state has constant total flux F through circles of constant θ:

$$F = \int_{\theta=cst} \boldsymbol{J} \cdot \hat{\boldsymbol{\theta}}\, \mathrm{d}s = \int J_{\hat{\theta}}\, \mathrm{d}s \tag{B.2}$$

with $\mathrm{d}s = R \sin\theta\, \mathrm{d}\phi$. The corresponding probability current is proportional to (ignoring factors of $\hbar$ and mass):

$$J_{\hat{\theta}} = \frac{1}{2\mathrm{i}} \left(\psi_l^{(+)m*} \partial_{\hat{\theta}} \psi_l^{(+)m} - \text{c.c.} \right). \tag{B.3}$$

The directional derivative is rewritten as

$$\partial_{\hat{\theta}} = \frac{1}{R}\frac{\partial}{\partial\theta} = -\frac{\sin\theta}{R}\frac{\partial}{\partial x}, \tag{B.4}$$

where $x = \cos\theta$. The current in terms of the Wronskian becomes

$$J_{\hat{\theta}} = \frac{2}{\pi R}\frac{\Gamma(l-m+1)}{\Gamma(l+m+1)} Wr\left(P_l^m, Q_l^m\right)\sin\theta \tag{B.5}$$

and hence the flux

$$F = 4\sin^2\theta\, Wr\left(P_l^m, Q_l^m\right)\frac{\Gamma(l-m+1)}{\Gamma(l+m+1)}. \tag{B.6}$$

Using the Wronskian [26] (p 145: formula (25) in chapter 3.4 for Legendre functions on the *cut*: $-1 \leqslant x \leqslant 1$):

$$Wr\left(P_l^m(x), Q_l^m(x)\right) = \frac{2^{2m}\Gamma\left(\frac{l+m+2}{2}\right)\Gamma\left(\frac{l+m+1}{2}\right)}{(1-x^2)\Gamma\left(\frac{l-m+2}{2}\right)\Gamma\left(\frac{l-m+1}{2}\right)} \tag{B.7}$$

with the duplication formula for the gamma function (A.10) for the numerator and denominator in (B.7) then gives

$$F = 4 > 0 \tag{B.8}$$

corresponding to an outgoing state. The constancy of the flux reflects probability conservation.

B.2. Semiclassical scattering states

As in appendix A we match the JWKB traveling states to the exact scattering states with the result

$$(a^2-x^2)^{-1/4}\exp\left(\pm\mathrm{i}\left(\frac{I_0}{\epsilon}-\frac{\pi}{4}\right)\right) \approx (-1)^m\sqrt{\frac{2l+1}{4\pi}}\pi\psi_l^{(\pm)m} \tag{B.9}$$

using (A.8) and

$$Q_l^m(0) = -2^{m-1}\pi^{1/2}\frac{\Gamma\left(\frac{l+m+1}{2}\right)}{\Gamma\left(\frac{l-m+2}{2}\right)}\sin\left(\frac{\pi}{2}(l+m)\right). \tag{B.10}$$

Hence, the scattering states lead to Dirichlet scattering phases given asymptotically by

$$-\frac{\psi_l^{(-)m}}{\psi_l^{(+)m}} \approx \exp\left(-\mathrm{i}\left(\frac{2I_0}{\epsilon}+\frac{\pi}{2}\right)\right) = \exp(-\mathrm{i}\Theta_m) \equiv S_m \tag{B.11}$$

with Θ_m given by (30) to leading order.

References

[1] Bracher C and Delos J B 2006 *Phys. Rev. Lett.* **96** 100404
[2] Friedlander F G 1975 *The Wave Equation on a Curved Space-time* (Cambridge: Cambridge University Press)
[3] Smilansky U 1994 *Les-Houches Summer School on Mesoscopic Quantum Physics* ed E Akkermans (Amsterdam: North-Holland) p 373
[4] Clairaut A C *et al* 1733 *Mem. Acad. Paris* p 86
[5] Spivak M 1979 *A Comprehensive Introduction to Differential Geometry* vol 3 (Boston, MA: Publish or perish)
[6] Abramovitz M and Stegun I 1972 *Handbook of Mathematical Functions* (New York: Dover)
[7] Edmonds A R 1974 *Angular Momentm in Quantum Mechanics* (Princeton, NJ: Princeton University Press)
[8] Backus G, Parker R and Constable C 1996 *Foundations of Geomagnetism* (Cambridge: Cambridge University Press)
[9] Dahlen F A and Tromp J 1998 *Theoretical Global Seismology* (Princeton, NJ: Princeton University Press)

[10] Brussaard P J and Tolhoek H A 1957 *Physica* **23** 955
[11] Bender C M and Orzag S A 1978 *Advanced Mathematical Methods for Sicentists and Engineers* (New York: McGraw-Hill)
[12] Gutkin B 2001 Billiards on surfaces of constant curvature *Thesis* Weizmann Institute of Science
[13] Smilansky U and Ussishkin I 1996 *J. Phys. A: Math. Gen.* **29** 2587
[14] Safarov Y and Vassiliev D 1992 *Spectral Theory of Operators (AMS Translations, Ser. 2* vol 150) ed S Gindikin (Providence, RI: American Mathematical Society)
[15] Creagh S and Littlejohn J D 1992 *J. Phys. A: Math. Gen.* **25** 1643
[16] Creagh S 1996 *Ann. Phys.* **248** 60
[17] Søndergaard N and Tanner G 2002 *Phys. Rev.* E **66** 066211
[18] Gutzwiller M C 1990 *Chaos in Classical and Quantum Mechanics* (New York: Springer)
[19] Brack M and Bhaduri R K 1997 *Semiclassical Physics* (Reading, MA: Addison-Wesley)
[20] Baltes H P and Hilf E R 1976 *Specta of Finite Systems* (Mannheim: Bibliographisches Institut)
[21] Colin de Verdière Y 1973 Spectre du laplacien et longueurs des gèodèsiques pèriodiques I, II *Compositio Math.* **27** 83–106
Colin de Verdière Y 1973 Spectre du laplacien et longueurs des gèodèsiques pèriodiques I, II *Compositio Math.* **27** 159–84
[22] Zelditch S 1997 *Geom. Funct. Anal.* **7** 145–213
Zelditch S 1998 *Geom. Funct. Anal.* **8** 179–217
[23] Zelditch S 2004 Inverse spectral problem for analytic domains: I. Balian–Bloch trace formula *Commun. Math. Phys.* **248** 357–407
[24] Colin de Verdiére Y 2005 *Ann. Henri Poincaré* **6** 925
[25] Fröman N and Fröman P O 1965 *JWKB Approximation: Contributions to the Theory* (Amsterdam: North-Holland)
[26] Erdéleyi A 1953 *Higher Transcendental Functions* vol 1 (New York: McGraw-Hill)
[27] Wirzba A 1999 *Phys. Rep.* **309** 1
[28] Ellegård C, Guhr T, Lindemann K, Lorensen H Q, Nygård J and Oxborrow M 1995 *Phys. Rev. Lett.* **75** 1546
[29] Ellegård C, Guhr T, Lindemann K, Nygård J and Oxborrow M 1996 *Phys. Rev. Lett.* **77** 4918
[30] Ellegård C, Schaadt K and Bertelsen B 2001 *Phys. Scr.* T **90** 223
[31] Couchman L, Ott E and Antonsen T M Jr 1992 *Phys. Rev.* A **46** 6193
[32] Bogomolny E and Hugues E 1998 *Phys. Rev.* E **57** 5404
[33] Kraus H 1967 *Thin Elastic Shells* (New York: Wiley)
[34] Wirzba A, Søndergaard N and Cvitanović P 2005 *Europhys. Lett.* **72** 534–40